Bidirectional DC/DC converter topology comparison and design

Texas Instruments

Zhong Ye
System Engineer

Sanatan Rajagopalan
Firmware Engineer

High Voltage Power Solutions
Texas Instruments

Learn about the basic design guidelines for bidirectional DC/DC converters in hard- and soft-switching modes.

A bidirectional direct current (DC)/DC converter is a key element of many new applications, such as automotive, server and renewable-energy systems. Low-voltage bidirectional DC/DC converters are usually nonisolated. All bidirectional converter designs or products currently on the market are based on the hard-switching synchronous buck topology. This paper uses an automotive 48-V/12-V bidirectional converter as an example with which to revisit the hard-switching synchronous buck topology and compare it to the transition-mode totem-pole zero-voltage-switching (ZVS) topology.

We used a digital controller to implement both hard- and soft-switching controls. A unique ZVS transition-mode control synchronizes multiple phases and maintains dead time cycle by cycle. We also designed and optimized two 110-A DC/DC converters for each topology in order to compare their performance, including efficiency and electromagnetic interference (EMI). Our results provide a guideline when designing bidirectional DC/DC converters to meet different cost, efficiency and EMI requirements.

Introduction

Many emerging applications require energy to be transferable between two ports bidirectionally. The two applications discussed in this paper using a low-voltage bidirectional DC/DC converter are a 48-V/12-V automotive dual-bus system and a server local energy storage (LES) system. These systems do not normally require isolation. For different systems, the reason and purpose for using bidirectional DC/DC converters can be quite different. With more and more electrification in automotive designs, the power demands for start-stop cars and micro-hybrid electric vehicles (HEVs) have increased significantly – approaching 3 kW of a 12-V power-supply limit.

A mild HEV demands much higher power. Over 200 A of current distributed on a 12-V bus requires a larger copper-wire cross-section, which increases system cost. Besides high-current-distribution conduction loss, 12-V high-power equipment becomes less efficient and has higher loss with increasing output power. To solve this issue, a 48-V power system is added to power the high-power components instead. **Table 1** shows an example of a BMW micro-HEV power-system change plan [1].

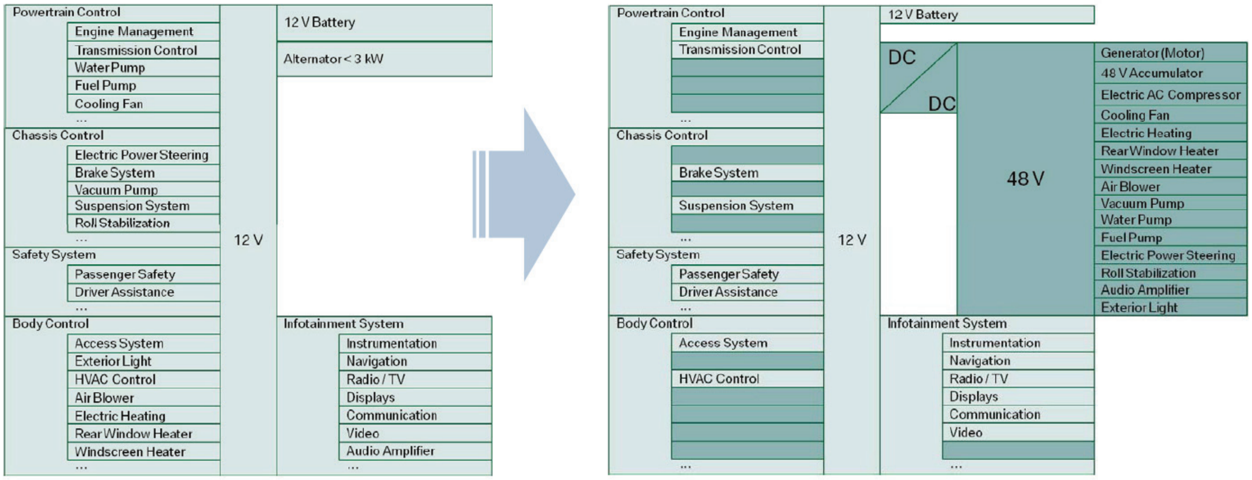

Table 1. *Displacement of high-power loads [1].*

Table courtesy of BMW.

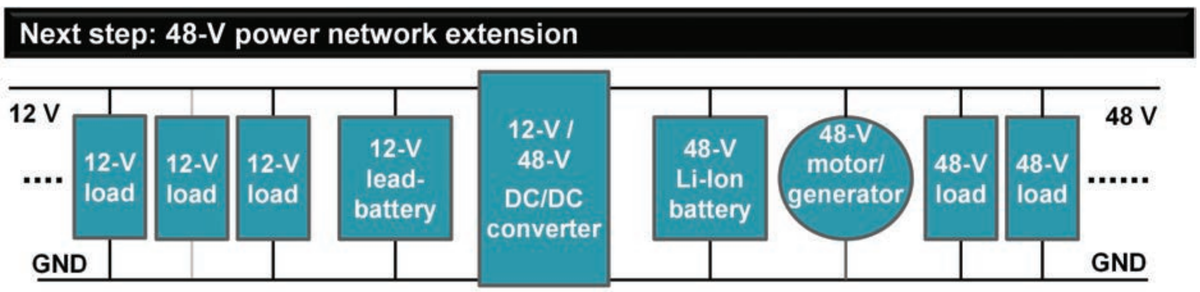

Figure 1. *A dual-bus power system for vehicle 12-V loads and 48-V loads.*

This power-system change plan eliminates the alternator and uses a bidirectional DC/DC converter powered by a 48-V bus to charge a 12-V battery (**Figure 1**).

A 48-V system has many advantages. For start-stop operation, recovering energy during braking or deceleration with 48 V is twice as efficient when compared to 12 V [1], [2], [3], [4], [5]. The recovered energy can provide supplemental power to accelerate the vehicle, enabling a driving system to gain fuel efficiency from downsized engines rather than losing engine performance. A 48-V system also confers the advantages of hybridization without the complexity while boosting overall fuel efficiency by 10 to 15 percent, which will help manufacturers meet increasingly stringent carbon-dioxide emission targets. The dual-bus architecture will remain valid until high-energy-density 48-V cold-cranking technology becomes practical, at which point manufacturers can switch all components to 48 V.

For servers and data centers, LES is a new power architecture designed to minimize backup-power footprints and reduce system cost while improving service availability. Microsoft initially proposed LES [6], but other industries quickly adopted it. Instead of using a centralized uninterruptable power supply (UPS), LES provides more reliable local backup power. **Figure 2** shows the differences between a traditional data center and a new data center with LES.

The simplicity of the LES design, coupled with its cost structure and service model, provide significant benefits for data-center deployments. LES eliminates up to 9 percent of the losses associated with conventional UPSs and frees around 25 percent of facility space.

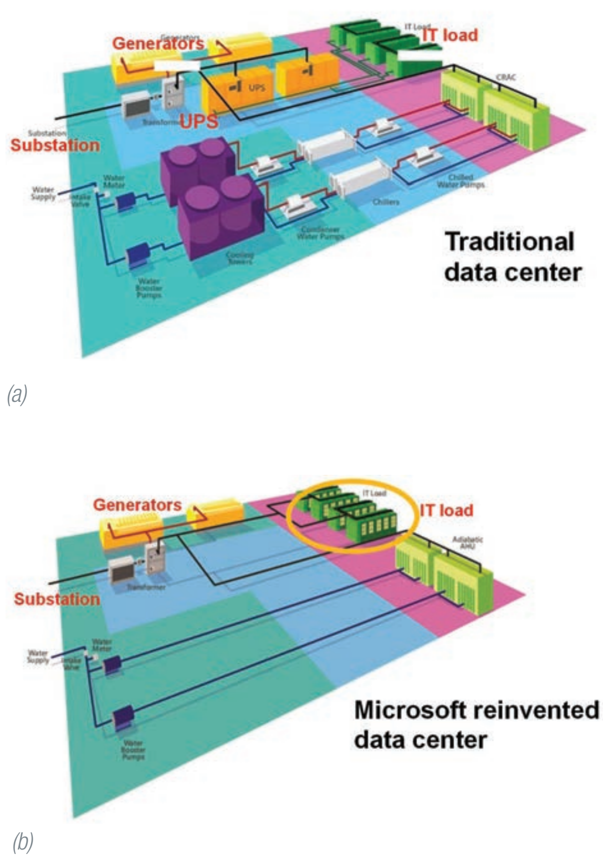

***Figure 2**. Traditional data center (a); Microsoft reinvented data center (b).*

A bidirectional DC/DC converter is also a key element of a server power supply with LES. When powered by an alternating current (AC)/DC rectifier output, a bidirectional DC/DC converter charges LES batteries during normal operation. The LES batteries provide backup power and regulate the AC/DC rectifier output voltage in the event of a power outage.

Bidirectional DC/DC converters have many applications and play an increasingly important role in energy recovery and power-system management. The most popular topology used for a converter design is a hard-switching synchronous buck converter, due to its circuit and control simplicity [7]. The other main topology is a ZVS transition-mode synchronous buck converter. This topology can operate in ZVS mode and has higher potential efficiency [8], [9], [10], [11]. Synchronous buck converters can operate in boost mode when you reverse their output currents.

For automotive applications, a multiphase interleaving structure avoids the need to use liquid or air cooling, increases the converter's power capacity, and distributes heat dissipation across a large area. Unlike a fixed-frequency hard-switching interleaved synchronous buck converter, a ZVS transition-mode interleaved buck converter operates in frequency-modulation mode. You must control its output inductor's negative current to limit the maximum switching frequency at light loads and provide the necessary energy for ZVS operation at heavy loads.

All phases must remain synchronized in any operational situation. Optimal and reliable control is complicated and still poses significant challenges for converter designers. This paper focuses on comparing the control implementation and performance of the two different topologies. We chose the UCD3138 digital controller for both hard-switching and ZVS control, and designed a four-phase 110-A/12-V power board to operate in both hard-switching and ZVS modes.

Topology and control

A single-phase bidirectional converter (**Figure 3**) can operate in buck mode and boost mode with hard-switching or ZVS operation. When Q_top is an active switch and Q_bot is a synchronous switch, the converter operates in buck mode (**Figure 4**); when the roles of Q_top and Q_bot reverse, the converter is in boost mode (**Figure 5**).

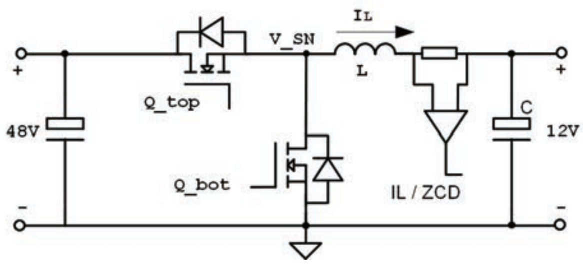

__Figure 3.__ A bidirectional converter power stage.

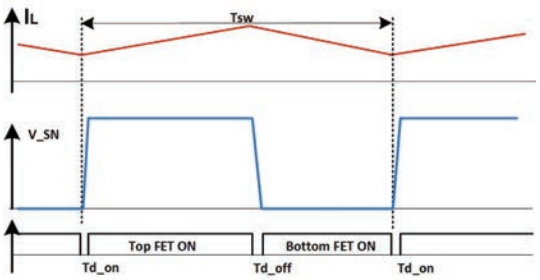

__Figure 4.__ Waveforms in hard-switching buck mode.

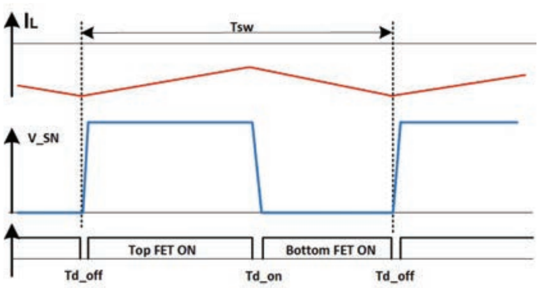

__Figure 5.__ Waveforms in hard-switching boost mode.

You can control the same buck converter to achieve ZVS by letting the inductor current become negative. When Q_top turns on in buck mode (**Figure 6**), the inductor current, IL, builds up linearly. When Q_top turns off, IL discharges switching node V_SN down. As long as the dead time Td_off is long enough, the bottom field-effect transistor (FET) Q_bot is able to achieve ZVS. However, excessive dead time results in a Q_bot body-diode conduction loss increase. Thus, turn on Q_bot as soon as V_SN discharges to zero.

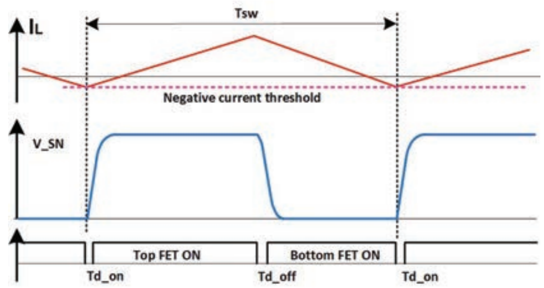

__Figure 6.__ Waveforms in ZVS buck mode.

Adaptive dead-time control minimizes switching and body-diode conduction losses. Equation 1 calculates the dead time Td_off as:

$$Td\_off = \frac{2 \cdot Coss\_tr \cdot V_{48}}{I\_pk} \qquad (1)$$

where Coss_tr is the equivalent capacitance of a metal-oxide semiconductor field-effect transistor (MOSFET) when Vds swings between 0 and V48, V48 is the voltage on the 48-V bus, and I_pk is the active switch Q_top turn-off current.

After Q_bot turns on, IL starts to decline. The switch stays on until the current reaches the predetermined negative current expressed as Equation 2:

$$I\_negative = \frac{2 \cdot Coss\_tr\,(V_{48} - 2 \cdot V_{12})}{Td\_on} \qquad (2)$$

where V12 is the voltage on the 12-V bus and Td_on is the dead time between when Q_bot turns off and Q_top turns on.

To achieve optimal operation, the dead time Td_on should be half the switch-node resonant period (Equation 3):

$$Td_{on} = \pi\sqrt{Lo \cdot Coss_{tr}} \qquad (3)$$

The energy stored in the output inductor is then just enough to charge the switch-node V_SN up to the V_{48} bus voltage, and Q_top can turn on with ZVS.

ZVS operation is also possible when operating in boost mode, as shown in **Figure 7**. The same control ideas apply to the negative-current calculation and dead-time control.

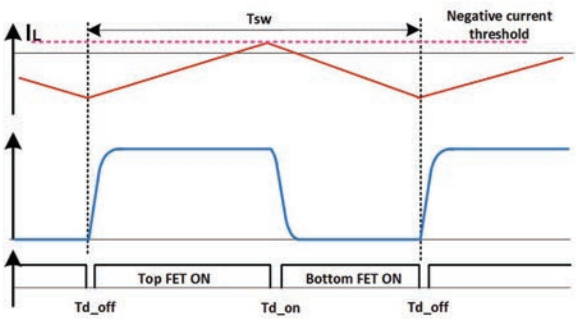

Figure 7. *Waveforms in ZVS boost mode.*

For a hard-switching bidirectional converter operating in continuous conduction mode (CCM), use adaptive dead-time Td_off control to achieve optimal efficiency but keep Td_on as small as possible.

Control implementation

The UCD3138 is a hybrid digital controller made up of three hardware digital loops and an ARM7 microcontroller [12]. The three digital loops can operate independently or in cascade mode. The controller architecture maintains the precision and high speed required for power processing while providing flexible power management.

A bidirectional DC/DC converter requires three loop controls. One is a current loop, and the other two are the V_{48} voltage loop and the V_{12} voltage loop. The controller's structure and peripherals match this bidirectional converter application perfectly.

Figure 8 shows a circuit block diagram of a controller-based bidirectional DC/DC converter.

One controller has eight digital pulse-width modulator (DPWM) outputs (four pairs), which can control four phases simultaneously. A shunt resistor senses each phase inductor current. All phase currents are summed together and connected to EADC0 for current-loop control.

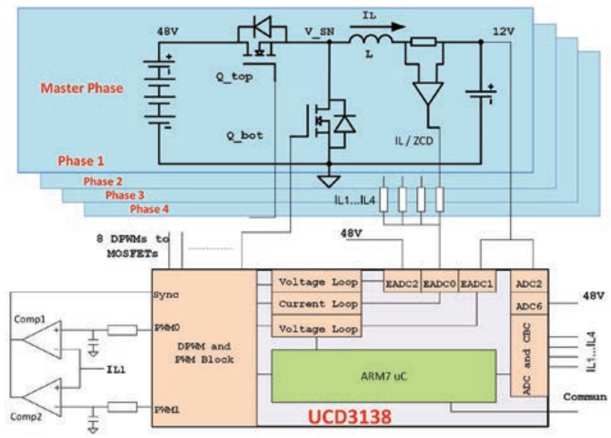

Figure 8. *Circuit block diagram of a bidirectional DC/DC converter.*

The 12-V and 48-V bus voltages are sensed and fed to EADC1 and EADC2 for voltage-loop control. Two general-purpose PWMs (PWM0 and PWM1) generate two programmable analog negative-current references and connect to compactor 1 and 2. One reference is for ZVS buck mode and the other is for ZVS boost mode. The comparators detect the master phase inductor's negative current. When the current reaches the reference threshold values, the comparator output, which connects to the UCD3138's sync pin, becomes high.

The rising edge of the signal at synchronous input forces the controller's DPWM to restart a new switching cycle and achieve hardware-based frequency modulation. All slave phases follow the master phase's frequency cycle by cycle. Each slave phase has a different delay time from the master phase. The ARM7 can modify the delay time, so all phases can maintain 90-degree interleaving when the switching frequency varies.

One important feature of the UCD3138 is that all dead times remain unchanged regardless of switching-frequency changes, while the ARM7 still has the privilege and flexibility to modify the dead time at any point.

A bidirectional DC/DC converter benefits from current-ripple cancellation of the interleaved structure. Selecting the right phase number can minimize or even fully cancel current ripple. For this specific case, where the high-voltage bus is 48 V and the low-voltage bus is 12 V, the voltage ratio is 4-to-1. The optimal phase number is thus a multiple of four.

Figure 9 shows the normalized current ripple versus the number of phases. You can see that for an ideal case, the inductor current ripple fully cancels out when the phase number is a multiple of four. It is for this reason that we used a four-phase bidirectional DC/DC converter to compare performance.

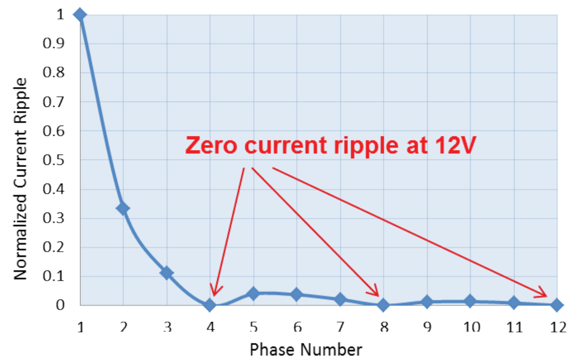

Figure 9. *Current ripple versus the number of phases.*

Design and test

To validate the control scheme and compare topology performance, we designed a 110-A (on the 12-V side) bidirectional DC/DC converter. When loaded with a different set of power components, the same design can operate in either hard-switching mode or ZVS mode. **Table 2** shows the power-stage component selection and design, and **Figure 10** shows the 110-A bidirectional DC/DC reference design.

Circuit parameters and components	Hard-switching	Soft-switching
Switching frequency	140 kHz	100 kHz-450 kHz
Current ripple at full load	16.25 A (±25% ripple)	65 A
Inductor value	4.7 uH	1.4 uH
Inductor DC resistance	1.86 mΩ	0.618 mΩ
Inductor part number	SER2915H-472KL (Coilcraft)	Litz wire: Strand AWG# 32, 110 strands PQ26/20 core -TDK B65877B0000R097
Inductor photos		
Main MOSFETs	Infineon IPB017N100N5: 100 V, 1.7 mΩ	Infineon IPB015N08N5: 80 V, 1.5 mΩ
Reverse protection FETs	CSD16556Q5B: TI, 20V, 1.062 mΩ @ 75°C	CSD16556Q5B: TI, 20 V, 1.062 mΩ @ 75°C
48-V fuses	Littlefuse: 0891030 30A, 2.06 mΩ @ 25°C, 2.18 mΩ @ 90°C	Littlefuse: 0891030 30 A, 2.06 mΩ @ 25°C, 2.18 mΩ @ 90°C
Low inductance shunt-sensing resistor	Panasonic ERJ-M1WTF2M0U: –2 mΩ	Panasonic ERJ-M1WTF2M0U: –2 mΩ
48-V input filter inductor	Coilcraft XAL1580-102 MEB: 1 uH 73.5 A, 0.93 mΩ typical	Coilcraft XAL1580-102 MEB: –1 uH 73.5A, 0.93 mΩ typical

Table 2. *Power-stage component selection and design.*

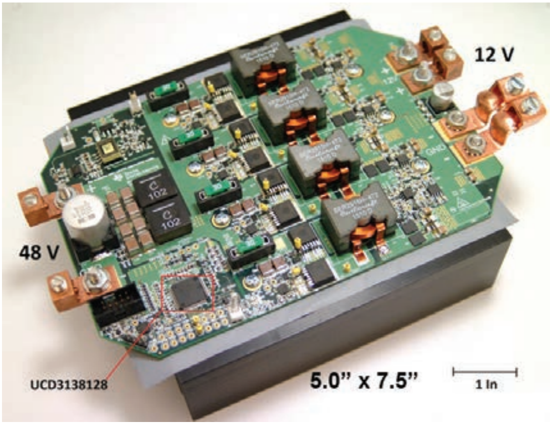

Figure 10. *Example of a 110-A (1.6-kW) bidirectional DC/DC converter.*

Figure 11 shows the switching-node voltage waveforms and inductor current waveform when the converter operates in ZVS buck mode. The switching-node waveforms are clean and soft, with a 90-degree phase offset from each other. The maximum frequency is clamped to 450 kHz. As the load decreases, the switching frequency increases. When the switching frequency reaches the 450-kHz limit, the negative current increases to prevent the switching frequency from increasing further.

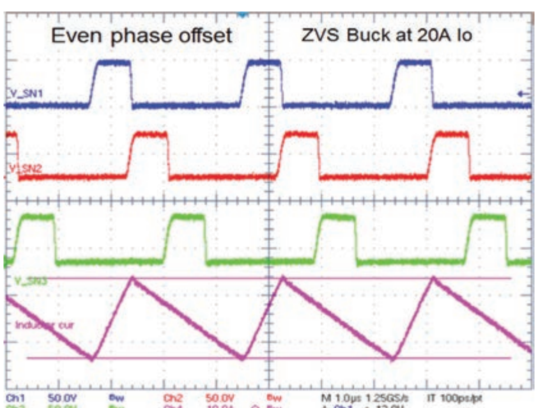

Figure 11. *Switching-node voltage and inductor-current waveforms in ZVS buck mode.*

Figures 12 through 19 show the difference between hard switching and soft switching. ZVS operation has softer voltage-rising and falling-edge waveforms, but you can still see some voltage overshoot when the MOSFETs turn off at a large current due to the printed circuit board (PCB) and power MOSFET pin leakage inductance. Hard-switching operation has a higher voltage overshoot. In addition to the PCB and MOSFET lead leakage, the MOSFET body diode’s reverse recovery contributes to overshoot and ringing as well.

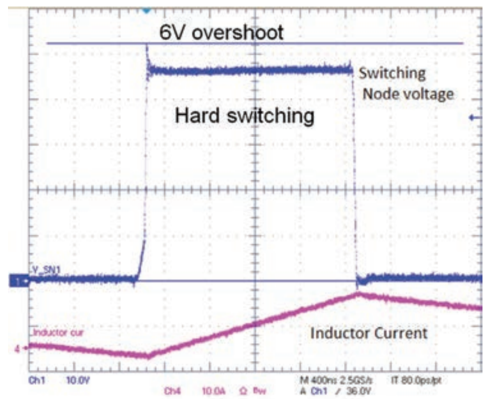

Figure 12. *Hard-switching buck at 20 A.*

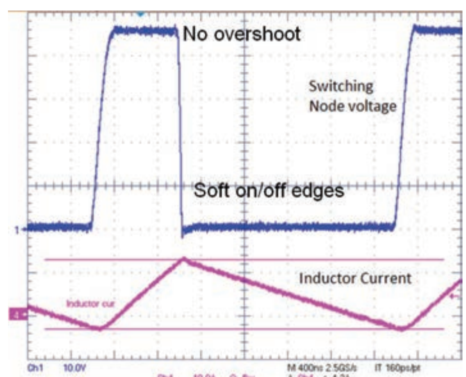

Figure 13. *Soft-switching buck at 20 A.*

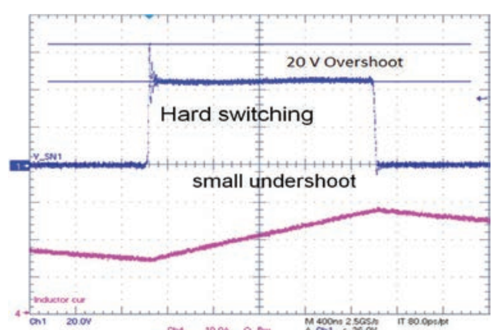

Figure 14. *Hard-switching buck at 110 A.*

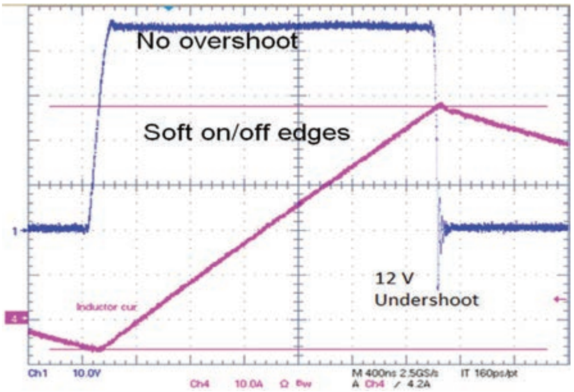

Figure 15. *Soft-switching buck at 110 A.*

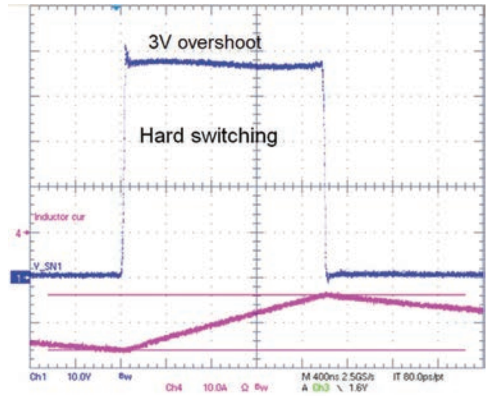

Figure 18. *Hard-switching boost at 110 A.*

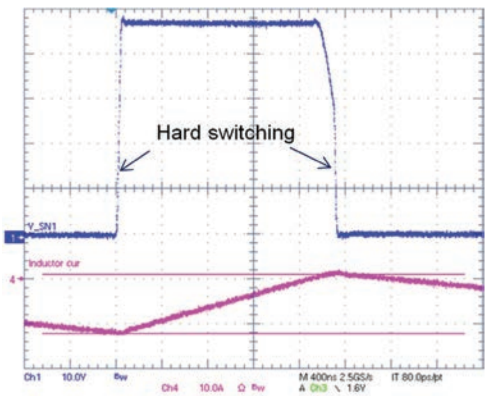

Figure 16. *Hard-switching boost at 20 A.*

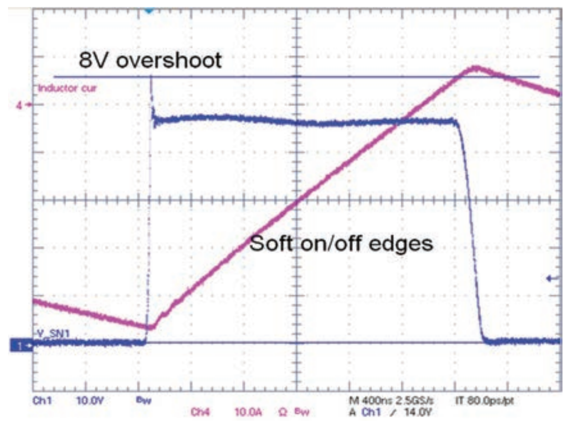

Figure 19. *Soft-switching boost at 110 A.*

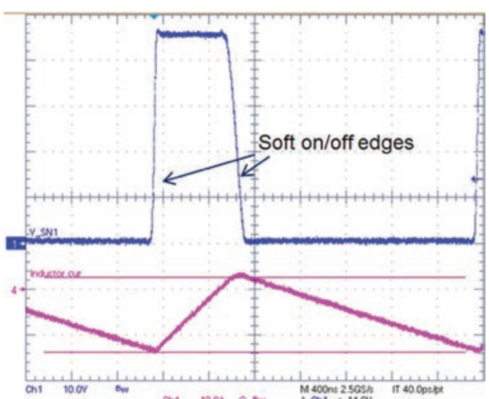

Figure 17. *Soft-switching boost at 20 A.*

Figure 20 shows the converter's bidirectional operation. The 12-V current ramps up and down between positive and negative values. When operating in buck mode, the current is positive and charges the 12-V battery. The current becomes negative in boost mode and the power from the 12-V battery charges up the 48-V battery.

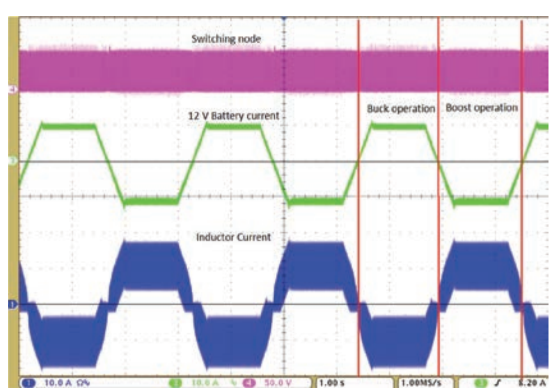

Figure 20. *Waveforms of bidirectional operation.*

A graphical user interface (GUI) tool (**Figure 21**) facilitates circuit debugging and tuning and handles operation monitoring (**Figure 22**).

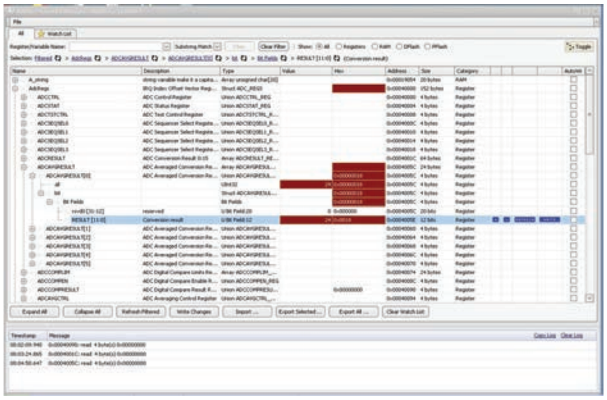

Figure 21. Device GUI for circuit debugging and tuning.

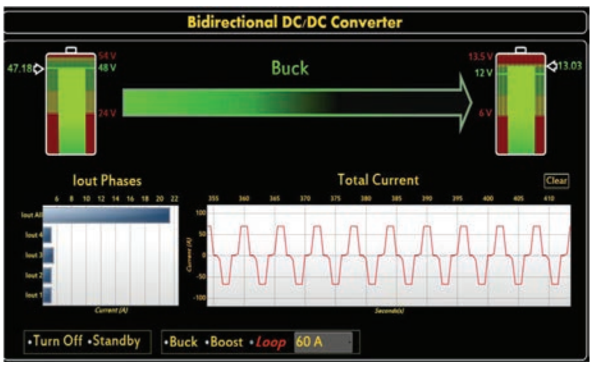

Figure 22. GUI for bidirectional DC/DC converter operation setting and monitoring.

We calculated the power losses of the reference design and charted the losses in the columns shown in **Figure 23**. You can see that the total loss of the converter with ZVS operation reduces, but the reduction is not significant. The major change is the power loss shifting from the MOSFETs to the inductors. This shift could be advantageous, since magnetic components are more reliable than semiconductors. Perhaps better magnetic materials could improve the ZVS converter's efficiency even further. **Figures 24** and **25** plot the converter's efficiencies versus loads.

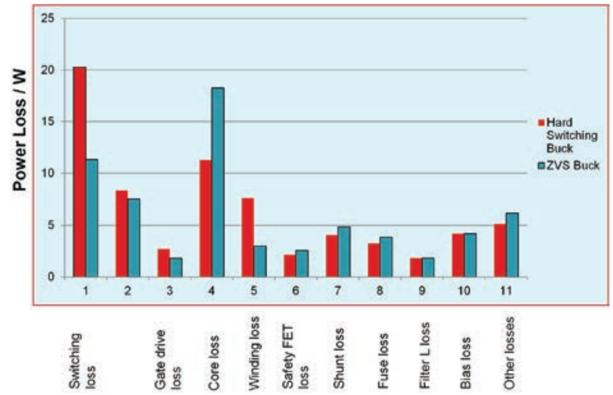

Figure 23. Loss breakdown of hard-switching and ZVS buck converters at full load.

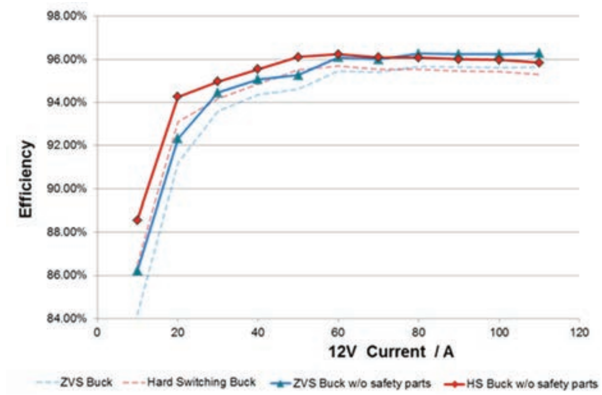

Figure 24. Efficiency versus load in buck mode.

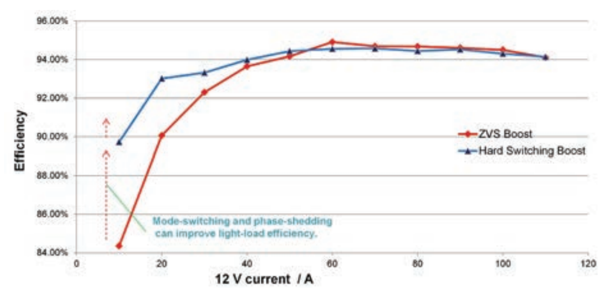

Figure 25. Efficiency versus load in boost mode.

In both buck and boost mode, hard switching has better light-load efficiency, while at heavy loads soft switching becomes more efficient. Soft switching still has turn-off loss. When the switching frequency increases at light loads, the loss becomes more significant.

We conducted additional tests with light-load management, which showed that disabling the synchronous FETs or using ideal diode-emulation control improved efficiency substantially. This project primarily focused on heavy loads where thermal performance is the major concern, but real product designs need light-load management.

Figures 26 through 29 show thermal images at full loads. We did not use any forced air for cooling, except a breeze from an electrostatic discharge (ESD) ion generator on top of the test bench to help stabilize the downfacing heat-sink temperature. From the thermal images, you can see that the MOSFETs' soft-switching temperature is lower than its hard-switching temperature in both buck and boost modes, and the overall soft-switching temperature is more even.

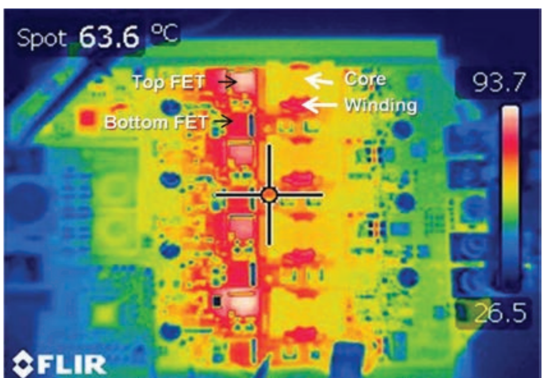

Top FET / C	Bottom FET / C	Core / C	Winding / C
84.75/92	68.25/69	64/65	77.5/78

Figure 26. *Hard-switching buck thermal image.*

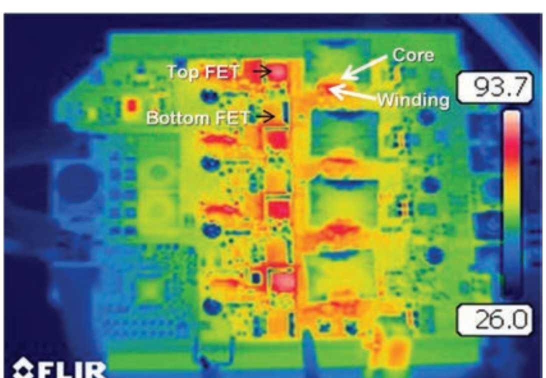

Top FET / C	Bottom FET / C	Core / C	Winding / C
72.0/73*	61.5/64	56.5//59	62.3//64

Figure 27. *Soft-switching buck thermal image.*

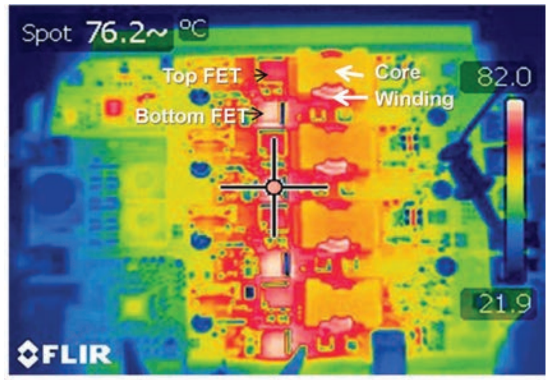

Top FET / C	Bottom FET / C	Core / C	Winding / C
67.25/72	75.25/77	63/64	69.25/73

Figure 28. *Hard-switching boost thermal image.*

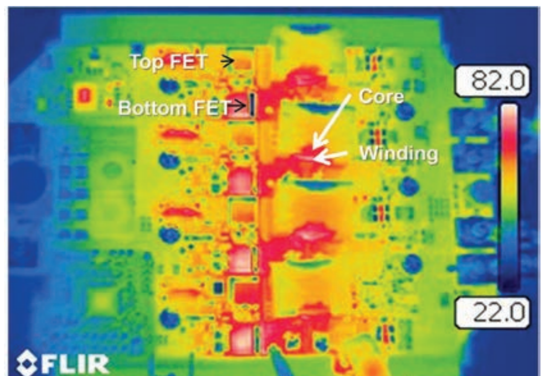

Top FET / C	Bottom FET / C	Core / C	Winding / C
64.3/66*	75.3/76	65/66	66.75/71

Figure 29.*Soft-switching boost thermal image.*

EMI is always one of the main concerns when selecting a topology. To have a reasonable comparison and better understand EMI behavior, we used the same EMI filter design on both the hard- and soft-switching converters and scanned the EMI in buck mode at full load. Test data in **Figure 30** indicates that soft switching and hard switching have no significant EMI difference under 1 MHz, but soft-switching's advantages become more substantial when the frequency increases. At 10 MHz and above, soft switching results in as much as a 15-dB reduction.

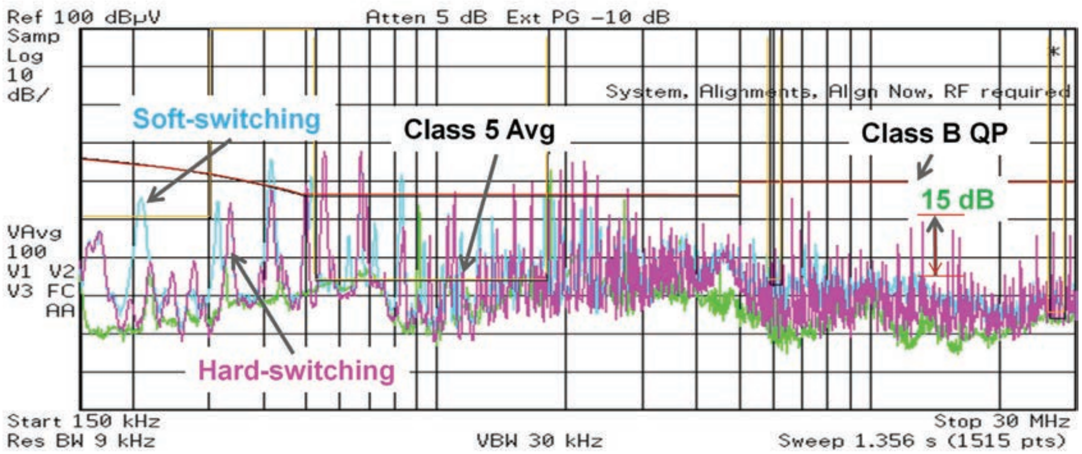

Figure 30. *Conducted EMI test of bidirectional DC/DC converters in buck mode at full load.*

Summary and conclusions

We designed and optimized two 110-A bidirectional DC/DC converters to compare performance in hard and soft switching and developed a GUI to facilitate circuit debugging, tuning and monitoring. Soft switching had softer and smoother switching-node waveforms and lower voltage overshoot. With no light-load management, hard switching is more efficient than soft switching at light loads, while soft switching has better efficiency at heavy loads.

The efficiency advantage of soft switching at heavy loads is not significant due to its large peak current and high turn-off loss, but its shift of losses from silicon to magnetic parts results in lower MOSFET temperatures and more even thermal distribution across the power board.

Light-load management can improve both soft- and hard-switching light-load efficiency. Soft switching does not exhibit a lower conducted EMI emission under 1 MHz, but its advantage becomes more significant with an increase in frequency and reaches 15-dB EMI reductions at 10 MHz and above.

Soft switching works better in general, but its design and control are more challenging. Topology selection for a design would depend on the specific requirements and the time and resources available.

The UCD3138 was a good fit for both the hard- and soft-switching bidirectional DC/DC converter designs. Its hybrid architecture offers precise and fast hardware power-processing control and flexible software power management. The controller’s hardware can support multiphase ZVS frequency modulation and maintain a constant dead time.

References

1. Sirch, O. “48 Volt – its threats and opportunities.” Automotive 48 V Power Supply Systems 2013 International Conference, Nov 12-14, 2013.
2. Harrop, P. “48 V vehicle systems becoming significant.” IDTechEx, Aug. 12, 2015.
3. “48V: Collected facts, latest developments and expert opinions.” Paper presented at 3rd International Conference Automotive 48 V Power Supply Systems 2015, Nov. 24-26, 2015.
4. “48V Technology on the Automotive Horizon.” Automotive IQ report presented at the 3rd International Conference Automotive 48 V Power Supply Systems 2015, Nov. 24-26, 2015.
5. Els, P. “48 Volt Electrification: The next step to achieving 2020 emissions.” Paper presented at 3rd International Conference Automotive 48 V Power Supply Systems 2015, Nov. 24-26, 2015.
6. Harris, S. “Microsoft Reinvents Datacenter Power Backup with New Open Compute Project Specification.” Microsoft Server & Cloud Blog, March 10, 2015.
7. Waffler, S., and J.W. Kolar. “Efficiency Optimization of an Automotive Multi-Phase Bi-directional DC-DC Converter.” 2009 IEEE 6th International Power Electronics and Motion Control Conference (IPEMC 2009) 574-581.
8. Zhang, J. “Bidirectional DC-DC Power Converter Design Optimization, Modeling and Control.” PhD diss, Virginia Polytechnic Institute, 2008.
9. Liqin, N., D.J. Patterson, and J.L. Hudgins. “High Power Current Sensorless Bidirectional 16-Phase Interleaved DC-DC Converter for Hybrid Vehicle Application.” IEEE Transactions on Power Electronics 27, No. 3 (2012) 1141-1151.
10. Yu, W., and J.S. Lai. “Ultra High Efficiency Bidirectional DC-DC Converter with Multi-Frequency Pulse Width Modulation.” Twenty-Third Annual IEEE Applied Power Electronics Conference and Exposition (APEC) (2008) 1079-1084.
11. Sah, A., K. Chaudhary, and V.V. Ratnam. “Non-Isolated Multiphase Buck-Boost Converter Design for Electric Vehicle Applications.” 2014 Annual International Conference on Emerging Research Areas: Magnetics, Machines and Drives (AICERA/iCMMD) (2014) 1-6.
12. UCD3138 Highly Integrated Digital Controller for Isolated Power. Texas Instruments data sheet (SLUSAP2F), November 2013

TI Worldwide Technical Support

Internet

TI Semiconductor Product Information Center Home Page
support.ti.com

TI E2E™ Community Home Page
e2e.ti.com

Product Information Centers

Americas	Phone	+1(512) 434-1560
Brazil	Phone	0800-891-2616
Mexico	Phone	0800-670-7544
	Fax	+1(972) 927-6377
	Internet/Email	support.ti.com/sc/pic/americas.htm

Europe, Middle East, and Africa

Phone

European Free Call	00800-ASK-TEXAS (00800 275 83927)
International	+49 (0) 8161 80 2121
Russian Support	+7 (4) 95 98 10 701

Note: The European Free Call (Toll Free) number is not active in all countries. If you have technical difficulty calling the free call number, please use the international number above.

Fax	+(49) (0) 8161 80 2045
Internet	www.ti.com/asktexas
Direct Email	asktexas@ti.com

Japan

Fax	International	+81-3-3344-5317
	Domestic	0120-81-0036
Internet/Email	International	support.ti.com/sc/pic/japan.htm
	Domestic	www.tij.co.jp/pic

Asia

Phone — Toll-Free Number

Note: Toll-free numbers may not support mobile and IP phones.

Australia	1-800-999-084
China	800-820-8682
Hong Kong	800-96-5941
India	000-800-100-8888
Indonesia	001-803-8861-1006
Korea	080-551-2804
Malaysia	1-800-80-3973
New Zealand	0800-446-934
Philippines	1-800-765-7404
Singapore	800-886-1028
Taiwan	0800-006800
Thailand	001-800-886-0010

International	+86-21-23073444
Fax	+86-21-23073686
Email	tiasia@ti.com or ti-china@ti.com
Internet	support.ti.com/sc/pic/asia.htm

A021014

Printed in U.S.A. by (Printer, City, State)

Texas Instruments

IMPORTANT NOTICE

Products		**Applications**	
Audio	www.ti.com/audio	Automotive and Transportation	www.ti.com/automotive
Amplifiers	amplifier.ti.com	Communications and Telecom	www.ti.com/communications
Data Converters	dataconverter.ti.com	Computers and Peripherals	www.ti.com/computers
DLP® Products	www.dlp.com	Consumer Electronics	www.ti.com/consumer-apps
DSP	dsp.ti.com	Energy and Lighting	www.ti.com/energy
Clocks and Timers	www.ti.com/clocks	Industrial	www.ti.com/industrial
Interface	interface.ti.com	Medical	www.ti.com/medical
Logic	logic.ti.com	Security	www.ti.com/security
Power Mgmt	power.ti.com	Space, Avionics and Defense	www.ti.com/space-avionics-defense
Microcontrollers	microcontroller.ti.com	Video and Imaging	www.ti.com/video
RFID	www.ti-rfid.com		
OMAP Applications Processors	www.ti.com/omap	**TI E2E Community**	e2e.ti.com
Wireless Connectivity	www.ti.com/wirelessconnectivity		

Mailing Address: Texas Instruments, Post Office Box 655303, Dallas, Texas 75265